Special Issue

UiO-66 and hcp UiO-66 Catalysts Synthesized from Ionic Liquids as Linker Precursors

Matthias Ermer,[a] Julian Mehler,[b] Björn Rosenberger,[a] Marcus Fischer,[a] Peter S. Schulz,[b] and Martin Hartmann*[a]

Using ionic liquids (ILs) as linker precursors, the well-known metal-organic framework (MOF) UiO-66 (Universitetet i Oslo) and the recently reported MOF **hcp** UiO-66 (hexagonal closed packed) have been successfully synthesized and characterized. The advantage of the applied novel synthesis approach is an economically and environmentally benign work-up procedure, due to the better solubility of the IL. Additionally, the reactivity of the terephthalate anions is increased compared to terephthalic acid, resulting in faster MOF formation with an increased amount of defects in the MOF structure. In order to explore to the influence of defects on the catalytic performance, the cyclisation of citronellal to isopulegol was employed as test reaction. The activity of **hcp** UiO-66 and **fcc** UiO-66 (face centered cubic) is improved compared to other MOF or zeolite based catalysts, while the selectivity is similar.

1. Introduction

During the last 20 years metal-organic frameworks (MOFs) have emerged as one of the most promising class of porous materials. MOFs are generally constructed of inorganic metal centers, which are connected by organic linkers.[1] Based on their unique and outstanding features, like their high modularity, the tremendous surface area and the large porosity, resulting in a capacity which is much higher compared to other porous materials,[2,3] these materials have received significant attention in recent years. Due to these features, metal-organic frameworks are regularly tested as promising candidates for various applications in catalysis,[4,5] gas storage[6] or gas separation.[7,8]

The amount of hypothetical MOFs, which can be synthesized, has been estimated to up to 138.000 different structures.[9] In general, the synthesis of these MOFs is very similar. Usually a solvothermal approach is used in which an inorganic metal salt and organic linkers are mixed in suitable organic solvents (e.g. N,N-dimethylformamide) and heated up for several hours in sealed reaction vessels at autogenous pressures or under reflux.[10,11] To circumvent the severe security risks, which arise from the used solvents that are commonly considered as hazardous, flammable or even both, Morris et al.[12] proposed the use of ionic liquids (ILs) as solvents and/or templates and introduced the term *ionothermal synthesis* for such a synthetic approach.

In recent years, ionothermal syntheses were used for the synthesis of new MOFs,[13] as well as prominent representatives such as MOF-5,[14] MIL-53[15] or ZIF-4.[16] However, several new MOFs have the disadvantage of having ions incorporated into the pores of the structure, resulting in de facto non-porous materials because their removal might result in a collapse of the framework.[17–19]

A prominent MOF that was synthesized ionothermally, is UiO-66 (Universitetet i Oslo),[20] which consists of $Zr_6O_4(OH)_4$ clusters. The triangular windows are capped alternatively by μ_3-OH and μ_3-O groups and the single clusters are connected with each other via the carboxylates of twelve terephthalate linkers. Therefore, different ILs were employed as solvent and/or structure directing agent resulting in pure UiO-66 or mixtures between **fcc** UiO-66 and **hcp** UiO-66.[21] Due to its high stability against thermal, physical and chemical stress, UiO-66 is considered a promising candidate for industrial applications.[22,23] It has been shown that defects play an important role for UiO-66.[24] In the case of UiO-66 two main defects are observed. On the one side, one or more terephthalate linkers that connect the zirconium oxide clusters are missing, which is generally termed missing linker defects.[23] The other type of defect is called missing cluster defect, describing the absence of whole clusters.[25] The on purpose introduction of defects has opened an independent field of research, known as defect engineering.[26] Beside the use of modulators like monocarboxylic acids,[27] a faster crystallization of the MOF also results in a higher amount of defects.[28] One way to speed up the crystallization process is to increase the amount of deprotonated terephthalate anions. For example, Zhao et al.

[a] M. Ermer, B. Rosenberger, Dr. M. Fischer, Prof. M. Hartmann
Erlangen Center for Interface Research and Catalysis (ECRC)
Egerlandstraße 3
91058 Erlangen (Germany)
E-mail: martin.hartmann@fau.de
[b] J. Mehler, Dr. P. S. Schulz
Chair of Chemical Reaction Engineering
Egerlandstr. 3
91058 Erlangen (Germany)

Supporting information for this article is available on the WWW under https://doi.org/10.1002/open.202000291

Special Issue *An invited contribution to a Special Issue dedicated to Material Synthesis in Ionic Liquids*

used this strategy by adding the base trimethylamine to the synthesis of UiO-66.[29]

Regardless of the type of defect, in both cases open metal sites are created at the neighboring metal clusters. For a missing linker defect two open metal sites are created, facing each other, whereas for a missing cluster defect, twelve open metal sites arise.[30] These open metal sites can act as Lewis acid sites turning UiO-66 into an efficient catalyst for a variety of reactions including the cross-aldol condensation[31] or the cyclisation of citronellal to isopulegol.[32] Due to a smaller crystal size, higher surface area and higher amount of defects, it was shown that ionothermal synthesized UiO-66 exhibits an improved catalytic activity compared to same material synthesized solvothermally in the Meerwein-Ponndorf-Verley reduction of 4-tert-butylcyclo-hexanone with isopropanol.[33] The possibility of using **hcp** UiO-66 as catalyst was also shown recently by Chen et al., who studied the ring opening of different epoxides with various alcohols. Their results indicated that **hcp** UiO-66 is more active than UiO-66, especially if **hcp** UiO-66 is prepared by transformation of UiO-66.[34] Furthermore, **hcp** UiO-66 was also used as catalyst in the tandem deacetalization Knoevenagel condensation, in which the activity of **hcp** UiO-66 was comparable to other MOFs (i.e. MIL-101-NH_2 or PCN-124) with respect to conversion.[35]

Based on these results, we here introduce a strategy for the ionothermal synthesis of UiO-66 by using ionic liquids as linker precursor. Using this strategy, we have shown in previous publications that some remarkable changes in the properties of MOFs such as MIL-53[36] or ZIF-4[16] occur. Additionally, we reported that the use of ILs as linker precursor can be advantageous for establishing an economical and environmentally benign process,[21] making MOFs more attractive for applications on an industrial scale. Here, we will show that this strategy leads to the successful syntheses of UiO-66 and **hcp** UiO-66 with outstanding high amounts of defects, due to an increased reaction rate that was investigated by observing the dampening of an ultrasound signal. Furthermore, the arising defects boost the catalytic activity of these MOFs in the cyclization of citronellal to isopulegol.

2. Results and Discussion

2.1. Synthesis and characterization of UiO-66 (IL) and hcp UiO-66 (IL)

UiO-66 and **hcp** UiO-66 were synthesized, using the IL $[PBu_3C_3H_6CN]_2[BDC]$ as linker precursor. To obtain a sufficient amount of UiO-66, a seven times numbered-up synthetic approach was used, based on the procedure, described in the experimental section. As evident from the XRD pattern, the syntheses with ILs as linker precursor were successful for both MOFs (Figure 1).

The characteristic reflections of UiO-66 for the (111) plane and the (200) plane are observed at 7.4° and 8.6°, respectively, in agreement with the simulated pattern. The ratio between intensity of the (111) reflection and the (200) reflection can be

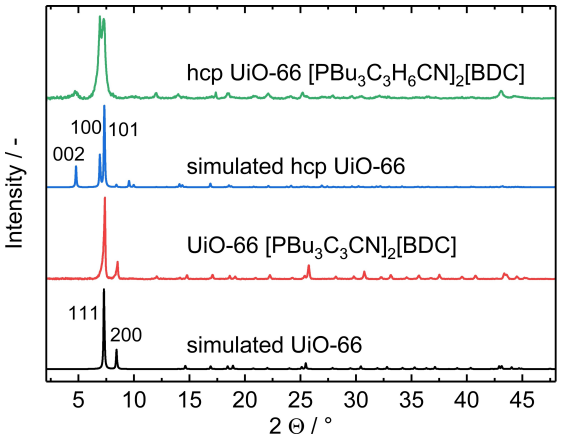

Figure 1. Normalized powder XRD pattern of UiO-66 simulated from the crystal structure published by Guillerm et al.[3] (black) and normalized PXRD pattern of UiO-66 synthesized with the IL $[PBu_3C_3H_6CN]_2[BDC]$ as linker precursor (red). For the simulated **hcp** UiO-66 the crystal structure from[21] was used (blue) and the experimental pattern with $[PBu_3C_3H_6CN]_2[BDC]$ as IL is shown in green.

used as an indicator for the orientation of UiO-66.[37] The comparison between the simulated pattern and the experimental one shows that the synthesized UiO-66 is nearly perfect orientated ($I_{111}/I_{200} = 4.5$ vs. 5.17). Furthermore no crystalline impurities (such as remaining terephthalic acid) are detected. Consequently, the use of ILs as linker precursor affords an environmentally-benign synthesis, because the generally essential extraction step in DMF for removing unreacted terephthalic acid is avoided. Probably this is a result of the better solubility of the anions compared to bare terephthalic acid. The same conclusion was drawn for the **hcp** UiO-66, however the characteristic reflections appear at $2\Theta = 4.7°$ ((002) plane), 7° ((100) plane) and 7.3° ((101) plane). Additionally, the reflections of **hcp** UiO-66 are less well pronounced compared to UiO-66, especially the one for the (002) plane, indicating that the **hcp** UiO-66 has a lower crystallinity than UiO-66.

The N_2 sorption isotherms of UiO-66 and **hcp** UiO-66 synthesized with $[PBu_3C_3H_6CN]_2[BDC]$ as linker precursor are shown in Figure 2. The shape of the isotherm of UiO-66 can be described as type I isotherm according to the IUPAC[38] classification, characterized by a steep uptake of nitrogen at low relative pressures resulting from micropore filling. At high relative pressures, interparticle condensation rather than an interpore condensation of nitrogen is observed, which results in hysteresis. However, below $p/p_0 = 0.5$, the isotherm is reversible. For UiO-66 a higher pore volume (0.68 $cm^3 g^{-1}$) and BET area (1673 $m^2 g^{-1}$) compared with the theoretically values (V_p = 0.43 $cm^3 g^{-1}$; $A_{BET} = 954\ m^2 g^{-1}$)[23] is calculated. The increased porosity can be explained by an increased amount of defects in the structure, probably resulting from a faster crystallization process during the synthesis with ILs as linker precursor (vide infra).

For **hcp** UiO-66, also a type I N_2 isotherm is obtained. During desorption, a hysteresis occurs that can be classified as H4 hysteresis with the typical forced closure at $p/p_0 = 0.48$, that is frequently observed for nitrogen as adsorptive.[39] For **hcp** UiO-

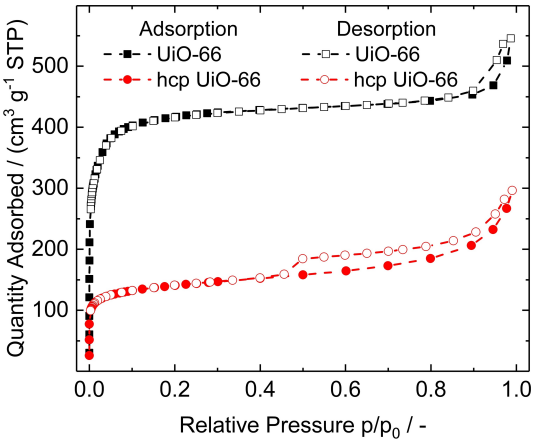

Figure 2. N_2 adsorption isotherms of UiO-66 (black, combined sample) and **hcp** UiO-66 (red) synthesized with $[PBu_3C_3H_6CN]_2[BDC]$. Filled symbols indicate the adsorption branches and empty symbols indicate the desorption branches.

66, a BET area of 528 $m^2 g^{-1}$ and a pore volume of 0.24 $cm^3 g^{-1}$ was calculated. These values are slightly lower compared to the theoretical ones (BET area 700 $m^2 g^{-1}$, pore volume 0.27 $cm^3 g^{-1}$) reported by Zhou et al.[40]

The absence of undesired non-crystalline impurities is further confirmed by ATR-FTIR measurements (Figure 3) for both MOFs. The most characteristic bands, which clearly can be ascribed to the ionic liquid, is the triplet of bands resulting from the stretching vibrations of the butyl groups located at wavenumbers 2957 cm^{-1}, 2927 cm^{-1} and 2864 cm^{-1}. None of these bands appear in the UiO-66 or **hcp** UiO-66 sample.

Furthermore, there is no indication for remaining DMF in the pores of UiO-66, which shows a characteristic band at 1667 cm^{-1} or unreacted terephthalic acid with a characteristic band at 1697 cm^{-1}.[22,41] Bands that appear in both MOFs are the doublet resulting from the stretching vibrations of the carboxylate groups located at 1581 cm^{-1} and 1390 cm^{-1}.[22] Compared to the IL, the band at 1390 cm^{-1} is shifted to higher wavenumbers, probably due to the coordination of terephthalate linkers to the metal clusters. According to Ma et al.,[42] the difference between the wavenumbers of the carboxylate bands contains some information about the bond character of the terephthalate linkers.

In the present cases, the difference is 188 cm^{-1}, indicating that the terephthalate can be considered as bridging ligand. A difference in the IR spectra between UiO-66 and **hcp** UiO-66 is observed in the finger print region at 554 cm^{-1} and 472 cm^{-1}, which is ascribed to the Zr–O bond vibrations. The band strength increases with the order of the metal clusters.[43] These bands are clearly visible for both MOFs, but stronger for **hcp** UiO-66. The same observation is made for the band at 3674 cm^{-1}, which is ascribed to the μ_3-OH groups. Since these groups are more frequent in **hcp** UiO-66, this circumstance is expectable. Moreover, water bonded via hydrogen bonds to the μ_2-OH groups in **hcp** UiO-66 gives rise to a band at 3650 cm^{-1}.[34] However, this band surprisingly also is found for UiO-66.

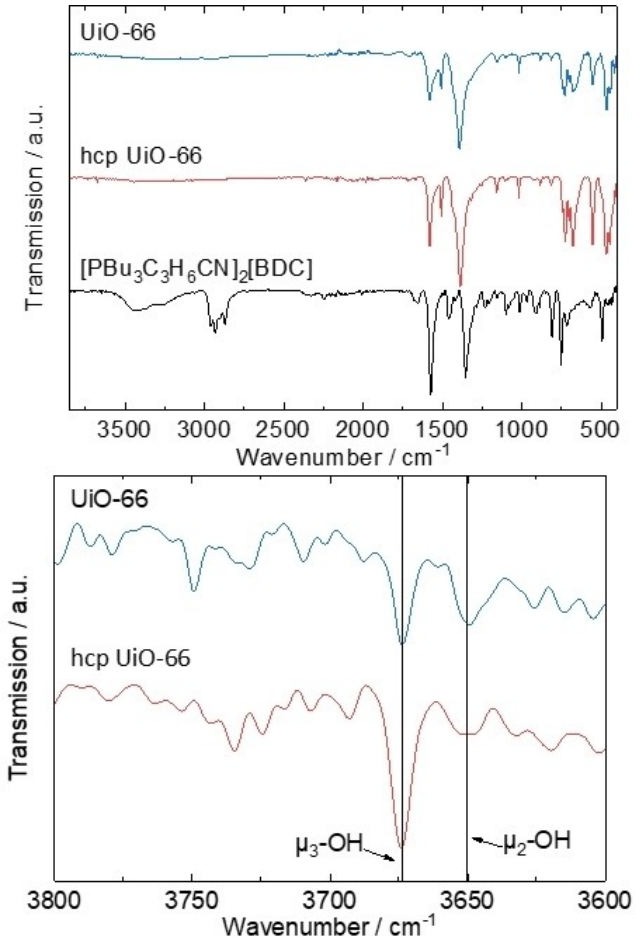

Figure 3. FTIR-spectra of UiO-66 (top, blue, numbered up), **hcp** UiO-66 (middle, red) and the IL $[PBu_3C_3H_6CN]_2[BDC]$ used as linker precursor (bottom, black). Below, a detailed view for the range from 3600 $cm^{-1}$to 3800 cm^{-1} is given.

To quantify the amount of missing linker defects, TGA measurements were performed. For UiO-66 the curve shows a mass loss at low temperatures until 373 K resulting from the loss of remaining solvent molecules (Figure 4). Around 473 K the dehydration of the metal clusters starts and finally a large weight loss of 46.4 wt.% occurs between 723 K and 790 K resulting from the decomposition of the structure. The theoretical value for the decomposition is 54.6 wt.%, thus on average four linkers are missing in each unit cell. As confirmed by powder XRD, exclusively ZrO_2 remains at temperatures above 800 K, which means that the mass is lower than theoretically expected. Therefore, missing cluster defects are assumed to be present in UiO-66.

Being fully aware of the limitations of the method, from a recalculation of the molecular formula, it can be roughly estimated that 3.5 zirconium atoms are missing in the unit cell, as well. For **hcp** UiO-66 the result looks somewhat similar, however the weight loss curve is broadened and the dehydration seems to be complete at around 593 K. The weight loss at the decomposition temperature amounts to 41.1 wt.%. Compared to the theoretical value, the experimental one differs by

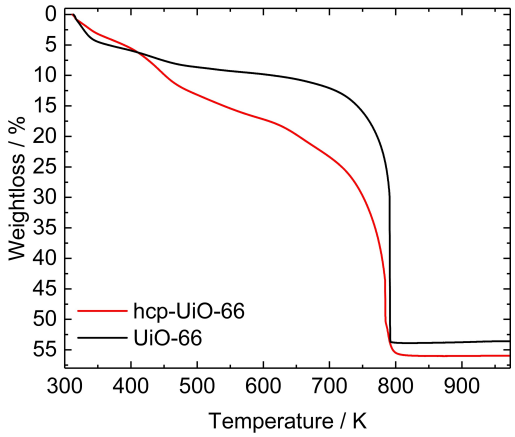

Figure 4. TGA measurements of UiO-66 (black) and **hcp** UiO-66 (red) synthesized with $[PBu_3C_3H_6CN]_2[BDC]$ as linker precursor.

9.3 wt.%, thus three linkers are missing. As for UiO-66, the remaining weight of the sample is again too low and using the same assumptions, roughly seven zirconium atoms are missing per unit cell in **hcp** UiO-66. This high amount of defects in the structure of **hcp** UiO-66 is rather surprising, since the BET area was even lower than the theoretical value and no pore blocking by impurities was detected.

UiO-66 crystallizes as well shaped octahedra as shown in the SEM (Figure 5). If the synthesis of UiO-66 is repeated several times, the shape of the crystals is similar, but the size of the particles largely varies from batch to batch. The majority of the particles is rather small with a size of just 70 nm. The next fraction has a size of around 200 nm and the large particles have a size of ca. 380 nm. Therefore, the reproducibility of the synthesis with respect to the particle size is rather low. However, from the current results it is unclear whether this is a consequence of the IL precursor or other parameters such as the used equipment (differences in the reaction vessels, heat distribution in the oven,…).

hcp UiO-66 (Figure 6) crystallizes in a very peculiar morphology, which is composed of intergrown platelets with 250 nm in diameter and a thickness of 25 nm in a desert rose type arrangement. In line with the PXRD results, the SEM image confirms, that the growth of the particles is rather less pronounced along the c-direction. However, the size of the **hcp** UiO-66 platelets is very similar. Similar morphologies are also observed for certain zeolites, e.g. ZSM-5, in the presence of special organic templates.[44]

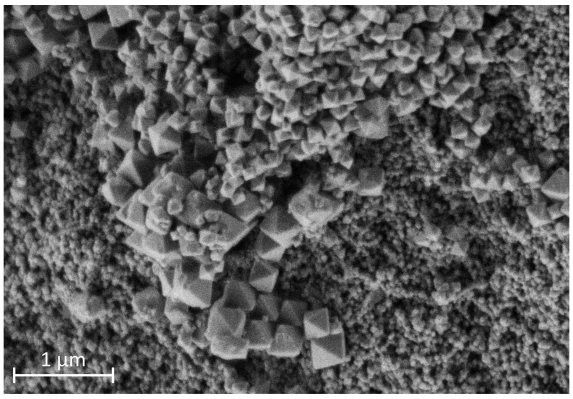

Figure 5. SEM image of UiO-66 synthesized with $[PBu_3C_3H_6CN]_2[BDC]$ as linker precursor.

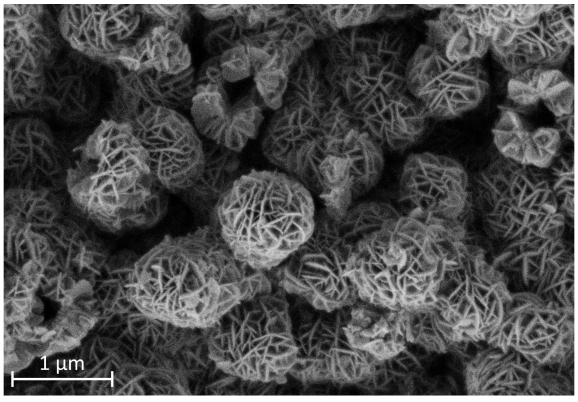

Figure 6. SEM image of **hcp** UiO-66, synthesized with $[PBu_3C_3H_6CN]_2[BDC]$ as linker precursor.

2.2. Results of the Catalytic Test Reaction

Due to the large surface area and the high amount of defects in both MOFs, it is expected that they are efficient catalysts for the cyclization of citronellal to isopulegol (Figure 7), which is catalysed by Lewis acid sites. Next to isopulegol, three other isomers are formed as products in the cyclization of citronellal (neo-, iso- and neoiso-isopulegol). Since only isopulegol has an industrial relevance as precursor in the synthetic production of menthol in the Takasago- and BASF- process, the selectivity of the MOF catalysts for isopulegol is crucial.[45–47]

Without a catalyst, citronellal is only converted into isopulegol in negligible amounts (Figure 8). This changes dramatically if one of the MOFs – UiO-66 or **hcp** UiO-66 – is added as a catalyst. For both MOFs the conversion increases, however, UiO-66 shows a higher conversion compared to **hcp** UiO-66 at any time. With regard to the composition of both MOFs, this result was rather unexpected. UiO-66 has a lower metal to linker ratio compared to **hcp** UiO-66. Since the zirconium centers are generally considered to be the active

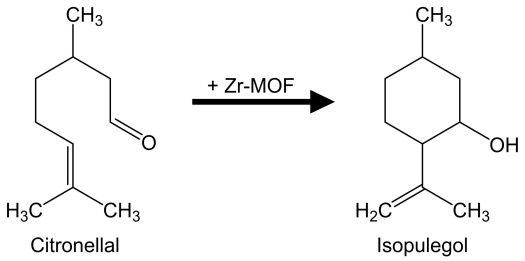

Figure 7. Reaction scheme of the cyclisation of citronellal to isopulegol.

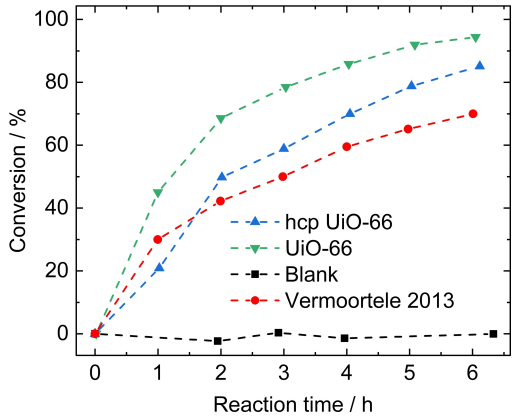

Figure 8. Conversion of citronellal to isopulegol with **hcp** UiO-66 (blue triangle) and UiO-66 (green triangle upside down) as catalyst. Additionally a blank experiment is added (black squares) and the data from[32] (red circles). The broken lines between the symbols are used to guide the eyes.

sites, **hcp** UiO-66 was expected to be catalytically more active. Additionally, it was recently suggested that the framework of **hcp** UiO-66 is advantageous for mass transfer, compared to the restricting small-pore windows allowing access to the pores of **fcc** UiO-66.[35] Due to the microporous nature of both MOFs, the transport of the reactant molecules within the frameworks is limited.[48] Additionally, the characterization of both MOFs revealed that the specific surface area of UiO-66 is roughly three times larger than that of **hcp** UiO-66. Consequently, **hcp** UiO-66 converts citronellal faster than UiO-66, if normalized to the BET area (assuming the same BET-area is available for citronellal than for N_2, ESI Figure S2). There might also be a decisive space limitation in the pores of **hcp** UiO-66. A general accepted reaction mechanism assumes that the linear citronellal molecule coordinates to the Lewis acidic catalytic center, where it gets initially shaped product-like. Afterwards, a C–C bond is formed by a nucleophilic attack of the C=C double bond to the carbonyl group and one hydrogen is transferred from one of the methyl groups to the carbonyl group.[49,50] In order for this mechanism to proceed, some space is required at the zirconium atom, which is why at least one linker should be missing and no additional modulator molecule should coordinate to the metal center.[50] Since it is known that at least water is still located around the additional bridging μ_2-OH groups of **hcp** UiO-66 after activation at 623 K,[34] it might be possible, that the activation of **hcp** UiO-66 at 593 K is not sufficient for a complete removal of all guest molecules. Consequently, these molecules might have a negative influence on the catalytic cyclization of citronellal to isopulegol, for example by simply reducing the required space.

Finally, to evaluate the rate of conversion, data from Vermoortele et al.,[32] who synthesized UiO-66 with different amounts of TFA (trifluoroacetic acid) to increase its catalytic activity, were added to Figure 8. Compared to UiO-66 prepared in the above mentioned study, the MOFs prepared in this study convert citronellal faster into isopulegol (Figure 8). Even the combination of TFA with HCl results in UiO-66 catalysts that exhibit a slower conversion compared to UiO-66 prepared in this study and in a similar one for **hcp** UiO-66 (ESI Figure S3).

The overall apparent activation energies of both MOFs are calculated to 61.4 kJmol^{-1} for **hcp** UiO-66 and to 62.5 kJmol^{-1} in case of UiO-66. A difference between both MOFs in the Arrhenius diagrams (ESI Figure S4) is the decreasing slope for **hcp** UiO-66 at higher reaction temperatures. This indicates, that at the chosen reaction conditions the conversion of citronellal to isopulegol at temperatures above 383 K starts to be limited by film diffusion.[48] Compared to the calculated activation energy in the gas phase (136.1 kJmol^{-1}),[49] both MOFs reduce the activation energy significantly in agreement with molecular modelling.[50]

For both MOFs a selectivity of roughly 72% to isopulegol is obtained (ESI Figure S5), which doesn't change with reaction temperature (Table 1). In addition to the other isopulegol isomers (neo-, iso- and neoiso-isopulegol), no further reaction products were detected. Similar selectivities are frequently observed, for example by Cirujano et al. who tested Cr^{3+}-MIL-101 and Pd@MIL-101 as catalysts.[51]

After the cyclization reaction, the MOFs were again characterized (ESI Figure S6 and Figure S7) by XRD and nitrogen sorption. and their recyclability in the cyclization reaction was tested. For the recyclability experiments, the MOFs were Soxhlet-extracted with ethanol after every cycle and dried in a convection oven prior to their activation. From the results (Figure 9) it can be concluded, that both MOFs can be reused for at least six times, however for **hcp** UiO-66, a significant loss of activity is observed. It, however, can not be ruled out that the work-up procedure has a significant influence on the catalytic activity of the MOF.[52] With exception of the second cycle, **hcp** UiO-66 shows a constant loss in activity between two cycles of 5.4%. In total, the **hcp** UiO-66 catalyst has lost about 50% of its activity after six cycles. Probably this is a result of the loss of crystallinity due the permanent impact of the stirring bar on the MOF during the catalysis, which is also reflected in the reduced BET area (436 m^{2}g^{-1}) (Figure S8). For the **fcc** UiO-66, the recyclability is much better, since its activity in the first and the sixth cycle is similar. However, neglecting the first cycle for the **fcc** UiO-66, the activity constantly decreases between two cycles by 3.2%. It is at present still an open question whether

Table 1. Overview about the catalytic parameters at different reaction temperatures. Conversion and selectivity were measure after a reaction time of 6 hours.

MOF	Temperature/K	k/s^{-1}	Selectivity*/%	Conversion*/%
UiO-66	363	0.0011	74.5	48.5
	383	0.0053	72.6	87.8
	393	0.0093	71.9	96.3
	398	0.0076	72.4	93.3
	403	0.0099	71.8	97.9
	408	0.0109	71.8	98.2
hcp UiO-66	363	0.0007	73.7	38.2
	373	0.0022	72.4	53.3
	383	0.0052	71.4	85.1
	393	0.0057	72.5	87.4
	398	0.0056	71.0	87.1
	403	0.0057	70.3	93.5

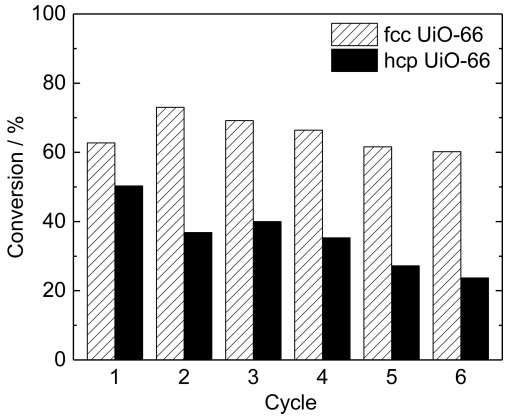

Figure 9. Recyclability of **fcc** UiO-66 and **hcp** UiO-66 as catalyst in the conversion of citronellal to isopulegol. For the recyclability experiments, freshly synthesized MOFs were used. The samples were taken after a reaction time of 6 h at a reaction temperature of 383 K and a stirring speed of 300 rpm.

this difference in recycling behavior of fcc UiO-66 and hcp UiO-66 is due to difference in defect concentration of the two catalysts. However, it is reported that these defects have no significant influence on the chemical and mechanical stability of UiO-66.,[2,52]

2.3. Crystallization Kinetics of UiO-66 with ILs as Linker Precursor

As shown so far, the use of ILs as linker precursors compared to H_2BDC results in an increased amount of defects in the frameworks, resulting in a larger BET area and a higher catalytic activity. As it is known, one way to introduce defects into crystals is a faster precipitation.[28] Therefore, it is assumed, that an increasing state of deprotonation of the terephthalate anions in the IL results in faster formation and growth of the MOF nuclei. To investigate this assumption, a glass reactor allowing to follow the crystallization process by the dampening of an ultrasound signal was used (Figure 10). Since this set-up is limited to reactions below the boiling point of the solvent, only the synthesis of **fcc** UiO-66 was studied. The resulting amplitude of the ultrasound signal with time is shown in Figure 10. The damping curve has a high signal to noise ratio due to several factors including the high amount of ions in the synthesis mixture and the differences in the densities of the solvent and the particles. Therefore, the obtained results were smoothed using the Savitzky Golay-method resulting in the curve that was used for further evaluation. From the smoothed curve it is evident that the formation and growth of nuclei starts immediately after the addition of the metal salt and is completed after approximately 250 min.

To determine the growth parameters, the Gualtieri model (1) was used, because it considers the nucleation and the growth as single processes.[53] Therein, the crystallization progress α depends on the elapsed time t, the dimensionality n of the growth, the rate constant for the crystal growth k_g and

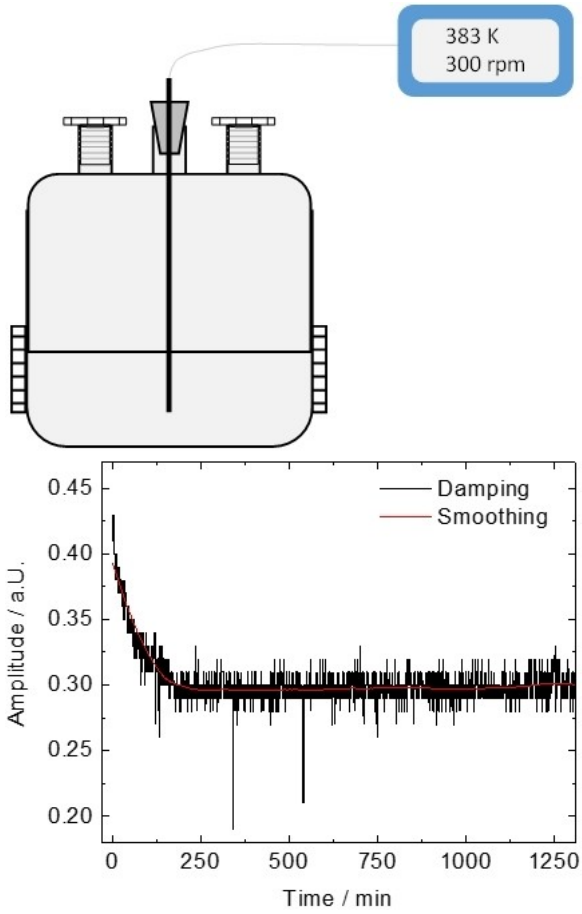

Figure 10. Schematic representation of the glass reactor, used for investigations of the crystallization kinetics of UiO-66 (top) and exemplary result for the damping of the signal during the nucleation and growth of the crystals (bottom). The black curve shows the damping for a reaction temperature of 383 K with [EMIM][HBDC] as linker source, the red curve shows the smoothed data using the Savitzky Golay-method at 600 points.

the parameters a and b expressing the nucleation. The dimensionality n of the **fcc** UiO-66 particles syntheses was found to be close to three, which is indicative of a phase boundary controlled reaction.

$$\alpha(t) = \frac{1}{1 + e^{-\frac{(t-a)}{b}}} \cdot \left[1 - e^{-(k_g t)^n}\right] \quad (1)$$

The good agreement of the model with the experimental data is shown exemplary in Figure 11 for the synthesis of **fcc** UiO-66 with [EMIM][HBDC] as linker precursor at 383 K. When conventional linker sources such as H_2BDC or Na_2BDC are used (Figure 11), the MOF formation is significantly slower. Using the one-fold deprotonated IL [EMIM][HBDC], the crystallization process at 373 K is already finished after 290 min and for the two-fold deprotonated one only after 480 min. The most likely explanation for this can be found with regard to the acid dissociation constants of acetic acid ($pK_a = 4.76$) and terephthalic acid ($pK_{a1} = 3.51$ and $pK_{a2} = 4.82$).[26] Here it must be noted that the values for the acidity constants refer to aqueous

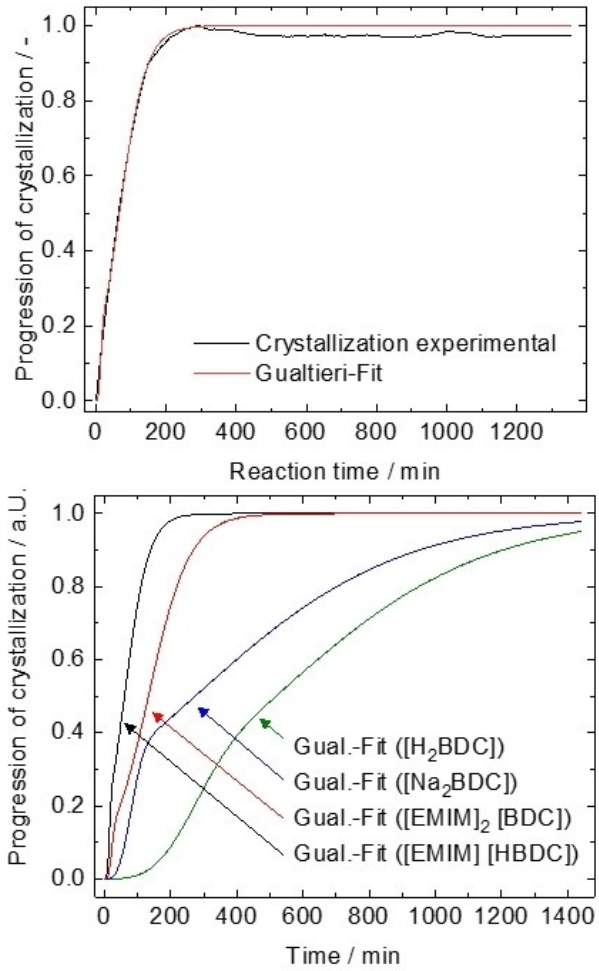

Figure 11. Representation of the experimental data for the crystallization progress for a UiO-66 synthesis using [EMIM][HBDC] as linker precursor (black) and the corresponding fit of the Gualtieri model (red) on the left side and the comparison between different linker sources on the right side at a reaction temperature of 373 K.

solutions, because of missing data for them in DMF. For a one-fold deprotonated terephthalate anion, the acidic strength of acetic acid is too low to reprotonate the anion. For a two-fold deprotonated terephthalate, it is likely, that such a reprotonation will occur. As a result, highly reactive acetate molecules exist in the reaction mixture if $[EMIM]_2[BDC]$ is used.

Consequently, their high reactivity slows down the crystallization process, resulting in a delayed formation of **fcc** UiO-66. Nonetheless, the reaction with $[EMIM]_2[BDC]$ as linker precursor is still much faster than with Na_2BDC. In the latter case, the crystallization process at 373 K is finished after more than 1400 min. This result indicates that not just the deprotonation of terephthalic acid is important, but also the cation has a decisive influence on the reaction rate. Regarding the nucleation and the growth of the particles separately (Figure S11), it becomes obvious, that the nucleation is much more effected by the cations. Whereas the growth differs rather little (but significantly), the nucleation is definitely speed up by the ILs. Additionally, the crystal growth seems to be the limiting step at the beginning of the reaction. Later the nucleation becomes rate limiting. For H_2BDC as linker source, this change is less obvious.

Additionally the rate constants and the apparent activation energies of the syntheses were calculated from Arrhenius diagrams (ESI Figures S12–15). For this purpose, syntheses were performed at different temperatures and the obtained constants were plotted logarithmically as a function of the inverse temperature. The rate constants for the nucleation k_n are obtained by equation 2. The single kinetic parameters are summarized in Table 2.

$$k_n = \frac{1}{a} \tag{2}$$

The results show, that the activation energies (Table 2) vary roughly between 45 kJ mol^{-1} and 112 kJ mol^{-1} for the growth and between 42 kJ mol^{-1} and 83 kJ mol^{-1} for the nucleation. In accordance with the results in Figure 11, the activation energies are in the order $H_2BDC > Na_2BDC > [EMIM]_2[BDC] >$ [EMIM][HBDC]. Beside the activation energies, the rate constants also confirm the results from Figure 11. Additionally, the rate constants for the growth k_g are always higher than those for the nucleation k_n. Therefore, the nucleation can be clearly identified as the rate limiting step, as it was already presumed a few times and it is in agreement with other publications.[54,55] The higer activation energies found here in comparison to earlier studies are probably a result of the additional stirring during the syntheses in this study. Indeed, if the stirrer speed is reduced to 100 rpm, the activation energies drop significantly (Figure S16). Finally, the values of the parameter b provide additional information about the nucleation. Since the values for b in Table 2 are bigger than 20, the nucleation seems to be an autocatalytic one.[53] However, the value for b decreases with increasing temperature, which is why the autocatalytic nucleation is transformed into a homogeneous ($b \approx 20$) or a heterogeneous ($b \leq 15$) one.

In summary, two conclusions are drown from the results of the crystallization study. First, the use of ILs as linker precursor decreases the activation energies, increases the rate constants and consequently speeds up the MOF-formation. Second, the state of deprotonation of the terephthalate anion influences the reaction rate remarkably in the current synthesis procedure, however an one-fold deprotonated terephthalate anion results in the highest nucleation rate.

3. Conclusions

We have shown that the concept of using ionic liquids as linker precursor can be used for the synthesis of the zirconium-based MOFs UiO-66 and **hcp** UiO-66. Both MOFs were obtained as pure phases. The advantage of using ILs as linker precursor is the possibility to skip the extraction step with DMF, due to the better solubility of the terephthalate anions compared to terephthalic acid. Therefore, a further step towards industrial scale applications was done by reducing the time, energy and chemicals consumed. The most remarkably difference between

Table 2. Kinetic parameters obtained from the Gualtieri model and Arrhenius plots. The time until the crystallization process is finished is termed with t_c.

Linker source	T/K	t_c/min	a/min	b/min	k_n/min^{-1}	k_g/min^{-1}	EA/kJ mol^{-1} k_g/k_n
H_2BDC	373	>1400	517	312	0.0019	0.0037	111.6/82.6
H_2BDC	383	1000	217	118	0.0046	0.0217	
H_2BDC	388	900	339	139	0.0030	0.0175	
H_2BDC	393	550	133	77	0.0075	0.0322	
H_2BDC	403	364	66	39	0.0151	0.0628	
Na_2BDC	373	>1400	273	309	0.0036	0.0114	95.4/72.8
Na_2BDC	383	646	142	95	0.0071	0.0250	
Na_2BDC	388	552	145	77	0.0069	0.0339	
Na_2BDC	393	374	93	53	0.0107	0.0470	
Na_2BDC	403	222	56	29	0.0179	0.0863	
[EMIM]	353	1096	195	170	0.0051	0.0253	45.3/42.1
[EMIM]	363	390	77	59	0.0130	0.0461	
[EMIM]	373	290	60	36	0.0167	0.0659	
[EMIM]	383	268	67	38	0.0149	0.0627	
[EMIM]	393	104	34	23	0.0294	0.1554	
$[EMIM]_2$	353	>1400	383	227	0.0026	0.0130	69.5/77.2
$[EMIM]_2$	363	932	285	122	0.0035	0.0283	
$[EMIM]_2$	373	480	132	62	0.0076	0.0436	
$[EMIM]_2$	383	230	59	32	0.0169	0.0767	
$[EMIM]_2$	393	110	29	15	0.0343	0.1612	

MOFs synthesized with ILs as linker precursor compared to their counterparts with terephthalic acid as linker source is the increased amount of defects and consequently an increased specific surface area. Due to presence of open metal sites, **fcc** UiO-66 and **hcp** UiO-66 are active catalysts in the cyclization of citronellal to isopulegol. Indeed, both MOFs showed a similar or higher activity compared to other published data from UiO-66 and their reuse was possible for six cycles. Additionally, the selectivity towards the main product isopulegol was high and didn't change with reaction time. Finally, the assumption that the higher amount of defects and the catalytic activity results from a faster precipitation/nucleation was confirmed by investigations of the crystallization process by measuring the dampening of an ultrasound signal. Using the Gualtieri model for the evaluation, it was clearly shown that the use of ILs as linker precursor accelerated the formation of UiO-66. In contrast to the initial assumption, the reaction rate did not rise with increasing deprotonation of the anions. Instead, an one-fold deprotonated terephthalate anion is most effective. Nonetheless, the faster crystallization could be ascribed to the use of ILs as linker precursor, provoked by a higher reactivity of the deprotonated terephthalate anions.

Experimental Section

Synthesis of 1-ethyl-3-methylimidazolium terephthalate ($[EMIM]_x[BDC]$)

A 100 mL Ace pressure tube was charged with 1-ethylimidazole (9.6 g, 100 mmol), dimethylcarbonate (36 g, 400 mmol) and 25 mL of methanol. The tube was sealed and the reaction mixture was stirred at 393 K for 24 h in an oil bath. The mixture was cooled to room temperature and slowly added to the respective amount of terephthalic acid in a 100 mL three necked flask. Strong foaming and gas evolution was observed. After stirring at room temperature overnight, excess MeOH and dimethylcarbonate were removed under reduced pressure. The white $[EMIM]_x[BDC]$ salts were collected, dried under vacuum and stored under argon. (Y-($[EMIM][BDC]$) = 27.5 g, >99%; Y($[EMIM]_2[BDC]$) = 19.231 g, >99%)

Synthesis of di-(tributyl-3-cyanopropylphosphonium) terephthalate ($[PBu_3C_3H_6CN]_2[BDC]$)

Under an inert gas atmosphere, tributylphosphine (97%, 29.22 g, 160 mmol) was dissolved in 100 mL of acetonitrile. 4-chlorobutyronitrile (97%, 15.57 g, 160 mmol), dissolved in 50 mL of acetonitrile, was added slowly, using common Schlenk techniques. Upon addition, the reaction mixture was stirred for 48 h under reflux. The solvent was removed under reduced pressure and the obtained crude chloride IL was washed three times with 50 mL of diethyl ether. For further purification, the ionic liquid was dried in vacuum at 333 K for three days and its purity was confirmed via ^{1}H, ^{13}C and ^{31}P NMR spectroscopy (45 g, 147.2 mmol, 92%). In a second step, an aqueous solution of $[PBu_3C_3H_6CN]Cl$ (0.5 M) was treated with an Amberlite IRN-78 anion exchange resin, to give a solution of $[PBu_3C_3H_6CN]OH$ (975 mL, 0,1325 M), which was subsequently neutralized with 10.7 g of terephthalic acid (64.6 mmol, 0.5 eq). H_2O was removed under reduced pressure and the remaining IL was further dried under vacuum at 333 K for 72 h. The product was obtained as a highly viscous, colorless liquid (Y-($[PBu_3C_3H_6CN]_2[BDC]$) = 45.5 g, 87.8%).

Synthesis of fcc UiO-66

For a typical synthesis of UiO-66, 0.28 g of $ZrCl_4$ (1.2 mmol) were dissolved in 40 ml of DMF (0.52 mol) in a 100 ml screw-cap bottle. Subsequently 6 ml of acetic acid (104.4 mmol) were added. Finally 0.54 g of di-(tributyl-3-cyanopropylphosphonium) terephthalate ($[PBu_3C_3H_6CN]_2[BDC]$) (0.72 mmol) were added to the clear solution and the sealed screw-cap bottle was placed in a preheated convection oven at 373 K for 24 h. After the reaction was terminated the mixture was cooled down to room temperature and the resulting white powder was separated from the liquid by centrifugation at 9000 rpm for 5 min and washed with technical ethanol. Finally UiO-66 was dried over night at room temperature and was Soxhlet-extracted with ethanol overnight to remove the

remaining DMF in the pores. In order to obtain sufficient material, the synthesis was repeated several times.

Synthesis of hcp UiO-66

In a typical synthesis, 0.84 g of $ZrCl_4$ (3.6 mmol) was dissolved in 60 ml of water (3.3 mol) in a 100 ml screw-cap bottle. Afterwards 18 ml of acetic acid (313.2 mmol) and 1.56 g of di-(tributyl-3-cyanopropylphosphonium)terephthalate ($[PBu_3C_3H_6CN]_2[BDC]$) (2.2 mmol) were added. The sealed screw-cap bottle was placed in a preheated convection oven at 373 K for 72 h. After the reaction time was expired, the sample was cooled down to room temperature. The resulting white powder was separated from the liquid by centrifugation at 9000 rpm for 5 min. The work-up procedure consisted of two washing steps with water followed by centrifugation. Finally the powder was dried at 373 K in a convection oven for approximately 24 h.

Synthesis of UiO-66 for US Damping Studies

H_2BDC as Linker Source

200 ml of DMF (2.6 mol) was submitted into a glass reactor, equipped with a transmitter and receiver for ultrasound damping, together with 6 ml of acetic acid (104.4 mmol) and 0.59 g of H_2BDC (3.5 mmol). The mixture was heated up to the reaction temperature (373 to 403 K) under stirring with 300 rpm. When the reaction temperature was reached, the addition of 0.8 g of $ZrCl_4$ (3.4 mmol) was used as starting point for the synthesis, which was recorded for a total of 24 h.

Na_2BDC as Linker Source

200 ml of DMF (2.6 mol) was submitted into a glass reactor, equipped with a transmitter and receiver for ultrasound damping, together with 30 ml of acetic acid (104.4 mmol) and 0.84 g of Na_2BDC (4 mmol). The mixture was heated up to the reaction temperature (373 to 403 K) under stirring with 300 rpm. When the reaction temperature was reached, the addition of 0.93 g of $ZrCl_4$ (4 mmol) was used as starting point for the synthesis, which was monitored up to 24 h.

[EMIM][HBDC] as Linker Source

200 ml of DMF (2.6 mol) was submitted to a glass reactor equipped with a transmitter and receiver for ultrasound damping, together with 30 ml of acetic acid (522 mmol) and 1.10 g [EMIM][HBDC] (4 mmol). The mixture was heated up to the reaction temperature (353 to 393 K) under stirring with 300 rpm. As the reaction temperature was reached, the addition of 0.93 g of $ZrCl_4$ (4 mmol) was used as starting point for the synthesis.

$[EMIM]_2$[BDC] as Linker Source

200 ml of DMF (2.6 mol) were submitted into a glass pot, equipped with a transmitter and receiver for ultrasound damping, together with 30 ml of acetic acid (522 mmol) and 1.55 g of $[EMIM]_2$[BDC] (4 mmol). The mixture was heated up to the reaction temperature (353 to 393 K) under stirring with 300 rpm. As the reaction temperature was reached, the addition of 0.93 g of $ZrCl_4$ (4 mmol) was used as starting point for the synthesis.

Catalytic Test Reaction

For the catalytic test reaction, 50 mg of catalyst and a stirring bar were placed in a 20 ml vial. The catalyst was activated under nitrogen atmosphere at 593 K overnight to remove residual solvent molecules from the pores. The still hot vial was sealed with a PTFE-coated butyl rubber septum immediately after it was removed from the calcination furnace. Afterwards, 5 ml toluene were added into the vial through the septum by using a syringe and the toluene/catalyst mixture was heated to the reaction temperature in an oil bath. After the reaction temperature was reached, the educt citronellal was added with a molar ratio of 15:1 with regard to the final amount of potentially catalytically active zirconium in the structure. The addition of citronellal marked the starting point of the reaction and right away a sample was taken from the reaction mixture and placed in a purification mixture based on 5 ml toluene and 50 μL n-Heptane as internal standard. The catalyst was removed from the purification mixture with a syringe filter and the sample was analyzed by gas chromatography employing a Shimadzu GC equipped with a FID detector and a FactorFour™ VF-WAXms (30 m × 0.25 mm × 0.25 μm) capillary column.

Characterization

All samples were characterized by powder XRD measurements using a PANalytical EMPYREAN diffractometer in Bragg-Brentano geometry equipped with a pixcel3D line detector. The copper X-ray tube providing CuKα1 (λ = 1.5406 Å) radiation was operated at 40 kV and 40 mA. The nitrogen adsorption isotherms were collected at 77 K on a Micromeritics ASAP 2000 instrument with micropore option. For the SEM pictures a Carl Zeiss ULTRA 55 field emission scanning electron microscope was used. The thermogravimetric analyses were performed with a SETSYS Evolution TGA© from SETARAM Instrumentation. The samples were heated with 2 K/min from 303 K to 973 K and air was used as carrier gas. For the infrared measurements, a Jasco FT/IR-4100 device equipped with a PIKE GladiATR accessory was used.

Acknowledgements

MH and PS gratefully acknowledge financial support by the "Deutsche Forschungsgemeinschaft" (DFG) within in the priority program SPP 1708 (Ha2527/14 and Schu2000/2).

Conflict of Interest

The authors declare no conflict of interest.

Keywords: UiO-66 · metal-organic frameworks · ionic liquids · US damping · citronellal cyclization

[1] R. E. Morris, L. Brammer, *Chem. Soc. Rev.* **2017**, *46*, 5444–5462.
[2] Y. Jiao, Y. Liu, G. Zhu, J. T. Hungerford, S. Bhattacharyya, R. P. Lively, D. S. Sholl, K. S. Walton, *J. Phys. Chem. C* **2017**, *121*, 23471–23479.
[3] V. Guillerm, S. Gross, C. Serre, T. Devic, M. Bauer, G. Férey, *Chem. Commun.* **2010**, *46*, 767–769.
[4] V. N. Panchenko, M. M. Matrosova, J. Jeon, J. W. Jun, M. N. Timofeeva, S. H. Jhung, *J. Catal.* **2014**, *316*, 251–259.
[5] M. Hartmann, M. Fischer, *Microporous Mesoporous Mater.* **2012**, *164*, 38–43.

[6] S. Chavan, J. G. Vitillo, D. Gianolio, O. Zavorotynska, B. Civalleri, S. Jakobsen, M. H. Nilsen, L. Valenzano, C. Lamberti, K. P. Lillerud, S. Bordiga, *Phys. Chem. Chem. Phys.* **2012**, *14*, 1614–1626.
[7] Q. Yang, A. D. Wiersum, H. Jobic, V. Guillerm, C. Serre, P. L. Llewellyn, G. Maurin, *J. Phys. Chem. C* **2011**, *115*, 13768–13774.
[8] U. Böhme, B. Barth, C. Paula, A. Kuhnt, W. Schwieger, A. Mundstock, J. R. Caro, M. Hartmann, *Langmuir* **2013**, *29*, 8592–8600.
[9] C. E. Wilmer, M. Leaf, C. Y. Lee, O. K. Farha, B. G. Hauser, J. T. Hupp, R. Q. Snurr, *Nat. Chem.* **2012**, *4*, 83.
[10] L.-M. Yang, E. Ganz, S. Svelle, M. Tilset, *J. Mater. Chem. C* **2014**, *2*, 7111–7125.
[11] M. Rubio-Martinez, C. Avci-Camur, A. W. Thornton, I. Imaz, D. Maspoch, M. R. Hill, *Chem. Soc. Rev.* **2017**, *46*, 3453–3480.
[12] E. R. Cooper, C. D. Andrews, P. S. Wheatley, P. B. Webb, P. Wormald, R. E. Morris, *Nature* **2004**, *430*, 1012–1016.
[13] T. P. Vaid, S. P. Kelley, R. D. Rogers, *IUCrJ* **2017**, *4*, 380–392.
[14] H.-M. Yang, L. Xian, X.-l. Song, T.-l. Yang, Z.-h. Liang, C.-m. Fan, *Trans. Nonferrous Met. Soc. China* **2015**, *25*, 3987–3994.
[15] M. Fischer, J. Schwegler, C. Paula, P. S. Schulz, M. Hartmann, *Dalton Trans.* **2016**, *45*, 18443–18446.
[16] M. Hovestadt, J. Schwegler, P. S. Schulz, M. Hartmann, *J. Chem. Phys.* **2018**, *148*, 193837.
[17] Q.-Y. Liu, Y.-L. Wang, N. Zhang, Y.-L. Jiang, J.-J. Wei, F. Luo, *Cryst. Growth Des.* **2011**, *11*, 3717–3720.
[18] Z. Lin, A. M. Slawin, R. E. Morris, *J. Am. Chem. Soc.* **2007**, *129*, 4880–4881.
[19] Q.-Y. Liu, W.-L. Xiong, C.-M. Liu, Y.-L. Wang, J.-J. Wei, Z.-J. Xiahou, L.-H. Xiong, *Inorg. Chem.* **2013**, *52*, 6773–6775.
[20] F. Joly, P. Devaux, T. Loiseau, M. Arab, B. Morel, C. Volkringer, *Microporous Mesoporous Mater.* **2019**, *288*, 109564.
[21] M. Ermer, J. Mehler, M. Kriesten, Y. S. Avadhut, P. S. Schulz, M. Hartmann, *Dalton Trans.* **2018**, *47*, 14426–14430.
[22] J. H. Cavka, S. Jakobsen, U. Olsbye, N. Guillou, C. Lamberti, S. Bordiga, K. P. Lillerud, *JACS* **2008**, *130*, 13850–13851.
[23] H. Wu, Y. S. Chua, V. Krungleviciute, M. Tyagi, P. Chen, T. Yildirim, W. Zhou, *JACS* **2013**, *135*, 10525–10532.
[24] Z. Fang, B. Bueken, D. E. De Vos, R. A. Fischer, *Angew. Chem. Int. Ed.* **2015**, *54*, 7234–7254.
[25] M. J. Cliffe, W. Wan, X. Zou, P. A. Chater, A. K. Kleppe, M. G. Tucker, H. Wilhelm, N. P. Funnell, F.-X. Coudert, A. L. Goodwin, *Nat. Commun.* **2014**, *5*, 4176.
[26] G. C. Shearer, S. Chavan, S. Bordiga, S. Svelle, U. Olsbye, K. P. Lillerud, *Chem. Mater.* **2016**, *28*, 3749–3761.
[27] A. Schaate, P. Roy, A. Godt, J. Lippke, F. Waltz, M. Wiebcke, P. Behrens, *Chem. Eur. J.* **2011**, *17*, 6643–6651.
[28] T. Lee, Y. H. Chang, H. L. Lee, *CrystEngComm*,**2017**, *19*, 426–441.
[29] Y. Zhao, Q. Zhang, Y. Li, R. Zhang, G. Lu, *ACS Appl. Mater. Interfaces* **2017**, *9*, 15079–15085.
[30] M. Taddei, *Coord. Chem. Rev.* **2017**, *343*, 1–24.
[31] F. Vermoortele, R. Ameloot, A. Vimont, C. Serre, D. De Vos, *Chem. Commun.* **2011**, *47*, 1521–1523.
[32] F. Vermoortele, B. Bueken, G. l. Le Bars, B. Van de Voorde, M. Vandichel, K. Houthoofd, A. Vimont, M. Daturi, M. Waroquier, V. Van Speybroeck, C. Kirschhock, D. E. de Vos, *J. Am. Chem. Soc,* **2013**, *135*, 11465–11468.
[33] X. Sang, J. Zhang, J. Xiang, J. Cui, L. Zheng, J. Zhang, Z. Wu, Z. Li, G. Mo, Y. Xu, *Nat. Commun.* **2017**, *8*, 1–7.
[34] X. Chen, Y. Lyu, Z. Wang, X. Qiao, B. C. Gates, D. Yang, *ACS Catal.* **2020**, *10*, 2906–2914.
[35] S. B. Peh, Y. Cheng, J. Zhang, Y. Wang, G. H. Chan, J. Wang, D. Zhao, *Dalton Trans.* **2019**, *48*, 7069–7073.
[36] J. Schwegler, M. Fischer, C. Paula, P. S. Schulz, M. Hartmann, *Chem. Ing. Tech.* **2017**, *89*, 887–893.
[37] M. Miyamoto, S. Kohmura, H. Iwatsuka, Y. Oumi, S. Uemiya, *CrystEngComm* **2015**, *17*, 3422–3425.
[38] M. Thommes, K. Kaneko, A. V. Neimark, J. P. Olivier, F. Rodriguez-Reinoso, J. Rouquerol, K. S. Sing, *Pure Appl. Chem.* **2015**, *87*, 1051–1069.
[39] J. C. Groen, L. A. Peffer, J. Pérez-Ramírez, *Microporous Mesoporous Mater.* **2003**, *60*, 1–17.
[40] L. Zhou, S. Wang, Y. Chen, C. Serre, *Microporous Mesoporous Mater.* **2019**, *290*, 109674.
[41] T. Loiseau, C. Serre, C. Huguenard, G. Fink, F. Taulelle, M. Henry, T. Bataille, G. Férey, *Chem. Eur. J.* **2004**, *10*, 1373–1382.
[42] G. Ye, D. Zhang, X. Li, K. Leng, W. Zhang, J. Ma, Y. Sun, W. Xu, S. Ma, *ACS Appl. Mater. Interfaces* **2017**, *9*, 34937–34943.
[43] L. A. Lozano, C. M. Iglesias, B. M. Faroldi, M. A. Ulla, J. M. Zamaro, *J. Mater. Sci.* **2018**, *53*, 1862–1873.
[44] V. R. Marthala, L. Urmoneit, Z. Zhou, A. G. Machoke, M. Schmiele, T. Unruh, W. Schwieger, M. Hartmann, *Dalton Trans.* **2017**, *46*, 4165–4169.
[45] B. Schäfer, *Chem. Unserer Zeit* **2013**, *47*, 174–182.
[46] J. Panten, H. Surburg, in *Ullmann's Encyclopedia of Industrial Chemistry* **2015**, pp. 1–9.
[47] S. M. Coman, P. Patil, S. Wuttke, E. Kemnitz, *Chem. Commun.* **2009**, 460–462.
[48] M. Hartmann, A. G. Machoke, W. Schwieger, *Chem. Soc. Rev.* **2016**, *45*, 3313–3330.
[49] M. Vandichel, F. Vermoortele, S. Cottenie, D. E. De Vos, M. Waroquier, V. Van Speybroeck, *J. Catal.* **2013**, *305*, 118–129.
[50] F. Vermoortele, M. Vandichel, B. Van de Voorde, R. Ameloot, M. Waroquier, V. Van Speybroeck, D. E. De Vos, *Angew. Chem. Int. Ed.* **2012**, *51*, 4887–4890.
[51] F. Cirujano, F. L. i Xamena, A. Corma, *Dalton Trans.* **2012**, *41*, 4249–4254.
[52] G. C. Shearer, S. Chavan, J. Ethiraj, J. G. Vitillo, S. Svelle, U. Olsbye, C. Lamberti, S. Bordiga, K. P. Lillerud, *Chem. Mater.* **2014**, *26*, 4068–4071.
[53] A. Gualtieri, *Phys. Chem. Miner.* **2001**, *28*, 719–728.
[54] F. Ragon, P. Horcajada, H. Chevreau, Y. K. Hwang, U.-H. Lee, S. R. Miller, T. Devic, J.-S. Chang, C. Serre, *Inorg. Chem.* **2014**, *53*, 2491–2500.
[55] F. Ragon, H. Chevreau, T. Devic, C. Serre, P. Horcajada, *Chem. Eur. J.* **2015**, *21*, 7135–7143.

Manuscript received: September 28, 2020
Revised manuscript received: November 12, 2020